

Corneal Strain Induced by Intracorneal Ring Segment Implantation Visualized With Optical Coherence Elastography

Journal Article**Author(s):**

Torres-Netto, Emilio A.; Kling, Sabine

Publication date:

2022-03

Permanent link:

<https://doi.org/10.3929/ethz-b-000539656>

Rights / license:

[In Copyright - Non-Commercial Use Permitted](#)

Originally published in:

Journal of Refractive Surgery 38(3), <https://doi.org/10.3928/1081597X-20211214-01>

Funding acknowledgement:

174113 - Measuring local corneal biomechanical properties by multi-frequency vibrography: Moving towards an earlier diagnosis of pathologies and personalized computer simulations (SNF)

1 **Corneal strain induced by intrastromal ring segment implantation visualized**
2 **with optical coherence elastography**

3 Emilio A. Torres-Netto^{1,2,3,4}, MD, PhD, Sabine Kling⁵, PhD

4

5 ¹ Laboratory of Ocular Cell Biology, Center for Applied Biotechnology and Molecular
6 Medicine, University of Zurich, Zurich, Switzerland

7 ² Faculty of Medicine, University of Geneva, Geneva, Switzerland

8 ³ Department of Ophthalmology, Paulista School of Medicine, Federal University of
9 Sao Paulo, Sao Paulo, Brazil

10 ⁴ Department of Ophthalmology, University Hospital Zurich, University of Zurich,
11 Zurich, Switzerland

12 ⁵ OPTIC team, Computer Vision Laboratory, ETH Zurich, Switzerland

13

14 **Word count:** 2365

15

16 **Corresponding author:**

17 Sabine Kling, OPTIC-team, Computer Vision Laboratory, Department of Information
18 Technology and Electrical Engineering, ETH Zurich, Sternwartstrasse 7, 8092 Zurich,
19 Switzerland, klings@ee.ethz.ch

20

21 **Financial disclosure:**

22 SK (none), ET (none)

23

24

25 **Abstract:**

26 **Purpose:** To record the axial strain field in the cornea directly after creating a stromal
27 tunnel and implanting an intracorneal ring segment (ICRS).

28 **Methods:** Freshly enucleated porcine eyes were obtained and assigned either to
29 ICRS implantation, tunnel creation only or virgin control. Immediately after manual
30 tunnel creation and ICRS positioning, the entire eye globe was mounted on a
31 customized holder and intraocular pressure (IOP) was adjusted to 15 mmHg. Then,
32 IOP was increased in steps of 1 mmHg to 20 mmHg and decreased again. At each
33 step, an optical coherence tomography volume scan was recorded. Displacements
34 between subsequent scans were retrieved using a vector-based phase difference
35 method. The induced corneal strain direction was determined by taking the axial
36 gradient. In addition, corneal surface was detected and sagittal curvature maps
37 computed.

38 **Results:** Corneal tissue presented a localized compressive strain in the direct vicinity
39 of the stromal tunnel, which was independent on IOP change. The central and
40 peripheral (exterior to the ICRS) cornea demonstrated compressive strains upon IOP
41 increase, and tensile strains upon IOP decrease. ICRS induced an annular shaped
42 tensile strain at its inner border, particularly during IOP increase. The compressive
43 strains close to the tunnel remained after ICRS implantation. Corneal curvature
44 changes were concentrated on regions where strain was induced.

45 **Conclusions:** ICRS implantation induces localized strains in the regions subjected to
46 refractive changes, suggesting that corneal strain and curvature are directly related.
47 Studying corneal strain in response to surgical intervention may provide new insights
48 on underlying working principles.

49 **Introduction:**

50 Intracorneal ring segments (ICRS) have been developed as a tool for refractive
51 correction in myopia¹, astigmatism² and especially corneal ectasias like keratoconus³.
52 ICRS have been designed to selectively flatten the cornea and consequently achieve
53 a refractive adjustment. Changes in corneal shape can be roughly predicted by the
54 Barraquer thickness law⁴: in order to achieve a similar refractive outcome, either an
55 equal amount of material could be theoretically removed from the central cornea or be
56 added to the corneal periphery. In this sense, additive surgery like ICRS implantation
57 is a technique of great potential as it permits a potentially permanent refractive
58 correction without introducing a structural weakening, such as with laser ablation. Yet,
59 the most important downside is that ICRS implantation remains poorly predictable.
60 Commercially available ICRS are typically made of polymethylmethacrylate and are
61 available in different dimensions with variations in thickness (150 to 350 μm), arc
62 length (90 to 240°), optical zone (5 or 6 mm diameter), base width (600 to 800 μm)
63 and cross-sectional shape (triangular, hexagonal, oval). Thicker rings with larger base
64 width and small optical zone are considered to induce the highest correction⁵, while
65 long arc lengths (>180°) are rather used for myopic correction and short arc lengths
66 for astigmatic corrections⁶.
67 Clinical studies have mainly assessed geometrical and refractive changes associated
68 with ICRS implantation^{3,7} and accordingly nomograms were created. Such
69 nomograms recommend ICRS dimension based on the location of the cone with
70 regard to a reference meridian. It has also been suggested that the keratoconus
71 phenotype visible on the refractive curvature map should be considered for ICRS
72 geometrical design and selection.⁸ Numerical studies have addressed ICRS
73 implantation from a more theoretical perspective. Especially parametric analyses are

74 helpful to disentangle the effect of different geometric and surgical factors.^{9–11}
75 However, these models often overestimate the achieved outcome, possibly because
76 the corneal material is not sufficiently well characterized, or because long-term post-
77 surgical processes such as epithelial or corneal remodeling have not been accounted
78 for.

79 We hypothesize that in order to better understand the underlying mechanisms of the
80 ICRS-induced refractive change, it would be fundamental to quantify the stress and
81 strain fields provoked by ICRS implantation. A recent numerical study evaluated the
82 change in corneal stress distribution after ICRS implantation⁹ and found that in the
83 anterior stroma stress relaxed, while in the posterior stroma stress increased.
84 Interestingly, the authors also showed that the ICRS implants were not able to stiffen
85 the cornea globally. In the direct surrounding of the implant, stress was reported to
86 have an uneven distribution, which was not further specified. Strain is the direct
87 (deformation) response of the cornea to a stress field induced either physiologically
88 through the intraocular pressure (IOP), or e.g. during refractive surgery. In an isotropic
89 material, strain is linearly related to stress, but even in an anisotropic material like the
90 cornea, the strain field is an important piece of information for mechanical
91 characterization. To the best of our knowledge, the strain field induced in response to
92 ICRS implantation has not been measured before.

93 Recently, we reported a novel technique^{12,13} to visualize corneal strain based on
94 optical coherence tomography (OCT) imaging and small-amplitude IOP modulation
95 that permits an evaluation of corneal biomechanics in a condition very close to the
96 eye's natural state. Applied to patterned corneal cross-linking,¹⁴ this approach was
97 able to detect a positive shift in strain limited to the irradiated (i.e. treated) area. While
98 this information is not only relevant for a better understanding of involved

99 biomechanical processes in refractive treatments, it might also be an indicator of
100 treatment success. The purpose of the current study was to experimentally quantify
101 the axial strain field that is induced during ICRS implantation at different steps of the
102 surgery.

103

104 **Methods:**

105 Implantation procedure

106 Freshly enucleated porcine eyes were obtained from the slaughterhouse and used
107 within 8 hours. The ICRS investigated in here had a triangular cross-section, a
108 thickness of 300 μm , an optical zone of 5 mm and did span over an arc length of 325°
109 (Keraring, Mediphacos Belo Horizonte, Minas Gerais, Brazil). This geometry was
110 chosen to guarantee a pronounced effect even in the porcine cornea, which is thicker
111 than the human cornea (878 μm ¹⁵ vs 515 μm ¹⁶) the ICRS was designed for.
112 Furthermore, a large arc length was taken to maximize the induced strains. Tunnel
113 creation was performed manually with dissectors dedicated for this purpose. The
114 control conditions consisted of (i) a full (360°) corneal tunnel only and (ii) a virgin
115 cornea.

116

117 Optical coherence elastography (OCE)

118 Imaging was conducted with a spectrometer based custom-built optical coherence
119 tomography system described earlier.^{12,14} Briefly, the system had an axial and lateral
120 resolution of 3.9 and 12.4 μm in tissue, respectively. The intraocular pressure (IOP)
121 was adjusted to 15 mmHg before the first measurement was taken. Subsequently, the
122 IOP was increased in steps of 1 mmHg from 15 to 20 mmHg and back to 15 mmHg
123 using a needle connected to a water column and a syringe. At each pressure step, a

124 volume scan consisting of 1000 x 100 A-scans spanning over an area of 10x10 mm
125 was recorded. Large scale motion (more than 1 pixel) between two subsequently
126 recorded volume scans was determined using a cross-correlation approach. Then
127 axially induced corneal strain was determined by calculating the axial gradient (in
128 direction of the OCT beam) of the phase difference between the two scans, following
129 a vector-based phase approach described in more detail earlier.^{12,14} In this context,
130 axial compressive strains (meaning tissue compaction) can be observed during IOP
131 increase and axial tensile strains (meaning tissue expansion / stretching) during IOP
132 decrease. Our previous study demonstrated¹² adequate controls with similar post-
133 mortem time are important when looking at comparisons of the strain profile.
134 Therefore, we paid attention that the different conditions were measured in close
135 temporal distance. Overall, the measurement of a single cornea took 5 min.

136

137 Curvature analysis

138 Surface detection of the anterior cornea was implemented by strongest reflection
139 tracking starting from the apex. The mean surface corresponding to an IOP between
140 15 and 20 mmHg was used for subsequent analyses. Next, the highest point of the
141 cornea was determined and corneal elevation centered on this point. Finally, sagittal
142 radius of curvature was computed and converted into dioptric power using a corneal
143 refractive index of 1.375.

144

145 **Results:**

146 Optical coherence elastography

147 **Figure 1** presents the cross-sectional view of the corneal structure and axial strain
148 during pressure increase and decrease. As expected, during pressure increase

149 corneas experienced compression resulting in negative axial strain and during
150 pressure decrease corneas recovered resulting in positive axial strain. The virgin
151 cornea demonstrated a homogenous strain distribution across the entire cornea (panel
152 a). Manual tunnel creation alone did cause localized compressive axial strain above
153 and below the cut (panel b), independent of pressure increase or decrease, while the
154 central portion of the cornea showed a similar response as the virgin cornea.

155 **Figure 2** presents corneal cross-sectional strain distribution after ICRS implantation
156 at different locations of the cornea. In the periphery – outside of the ICRS – the tissue
157 showed similar compressive and tensile behavior as the virgin cornea. In the direct
158 vicinity of the corneal tunnel (panel a), the compressive strain was similar to the cornea
159 with tunnel creation only. At the outer edge of the ICRS (panel b), during IOP increase
160 the implant induced tensile strain located under the bottom corners, which got further
161 enhanced during IOP decrease. Furthermore, compressive strain was induced at the
162 peak of the ICRS, particularly during IOP increase. At approx. $\frac{1}{4}$ of the ICRS (panel
163 c), the implant caused tensile strain in the anterior cornea, precisely coinciding with
164 the region between the two arcs of the ICRS, both during IOP increase and decrease.
165 Towards the center of the ICRS where the distance between the arcs were higher
166 (panel d), the implant induced localized tensile strains, which were predominantly
167 located in the posterior cornea. The central anterior cornea presented compressive
168 strain during IOP increase, which however did not fully recover during IOP decrease.

169 **Figure 3** shows the corresponding enface view of corneal structure and axial strain
170 during pressure increase and decrease. The compressive strain in the vicinity of the
171 tunnel is visible along its entire length. After ICRS implantation (panel c), during IOP
172 increase a second ring of positive strain (red color) became visible at the inner edge
173 of the ICRS, indicating a region of localized tissue relaxation. During IOP decrease

174 mostly positive strains were observed, hence localized relaxation due to ICRS
175 implantation is visible with less contrast. Notably however, after ICRS implantation the
176 strain amplitude in the center was higher than in virgin and tunnel-only controls. **Table**
177 **1** summarizes the axial strain distribution in the cornea observed with the different
178 conditions.

179 Axial strain profile

180 **Figure 4** presents the axial strain profile during IOP increase in the most central optical
181 zone of 2 mm diameter as well as the corresponding axial displacement as a function
182 of IOP. During IOP increase (panel a), central corneal strain in virgin and tunnel-only
183 corneas were similar and tended to have small negative values (indicating
184 compression) throughout the whole cornea. In contrast, corneas with an ICRS
185 implanted presented a pronounced – yet not significant – positive axial strain
186 (relaxation) in the posterior 20% of the tissue. During IOP decrease (panel b), corneal
187 strain values were generally larger and had positive sign, except in the anterior 10%
188 of the cornea where negative strains were observed. Similar to IOP increase, after
189 ICRS implantation the posterior 20% of the cornea demonstrated significantly higher
190 positive strain values than virgin or tunnel-only corneas (at 850 μ m depth: virgin vs
191 ICRS, $p=0.003$; tunnel-only vs ICRS, $p=0.026$) indicating stronger posterior relaxation
192 with ICRS. Axial displacement (panel c) was largest in the virgin cornea and smallest
193 after ICRS implantation. Noticeably, the induced deformation during IOP modulation
194 was mostly reversible in the cornea with ICRS, however all conditions demonstrated
195 a hysteresis. Hysteresis in this context refers to the remaining deformation after IOP
196 modulation, which was assessed the second time an IOP of 15 mmHg was reached
197 (accumulated deformation in panel C).

198 Curvature analysis

199 **Figure 5** presents the sagittal curvature map of the cornea before and after ICRS
200 implantation. Tunnel creation alone (panel a) left corneal curvature unaffected
201 (41.1 ± 2.1 diopters), except for few localized aberrations. After ICRS implantation
202 (panel b) a pronounced decrease in corneal curvature to 21.8 ± 9.0 diopters was
203 observed inside the ICRS implantation area, which went along with a ring of curvature
204 increase to 53.5 ± 8.9 diopters located in the periphery, outside of the ICRS
205 implantation. Interestingly, the region that flattened most did match surprisingly well
206 with the region in which localized strain alterations were observed, compare dashed
207 reference circles in Figures 3 and 5.

208

209 **Discussion:**

210 We report for the first-time corneal strain alterations resulting from ICRS implantation
211 measured under close-to-physiologic loading conditions. We demonstrate that
212 localized corneal curvature changes are mostly restricted to the region in which
213 corneal strain is induced. This observation is in line with previous literature suggesting
214 that the regularizing effect of an ICRS on the cornea is attributed to local bulking rather
215 than globalized stiffening.⁹ The observed annular region of positive strain that was
216 induced interior to the ICRS corresponds to the predicted relaxation of the anterior
217 cornea in simulations⁹. The corneal strain profile demonstrated that in the central
218 tissue posterior relaxation was even more dominant. Due to the positive sign of strains
219 induced by the ICRS, differences were more apparent in OCT images during IOP
220 increase (global stressing) than decrease (global relaxation). Overall, the location of
221 ICRS-based strains matched well with the observed sagittal curvature changes
222 suggesting that corneal strain amplitude and curvature were directly related.
223 Interestingly, the induced displacement was more reversible after ICRS implantation.

224 This was likely a result of the ICRS reducing corneal strain by taking up part of the
225 applied stress, which results in shifting the physiologic state towards the left (i.e.
226 towards the linear elastic region) in the stress-strain diagram and reducing the risk of
227 plastic deformation. In the end, these observations suggest that corneal tissue interior
228 to a 325° arc length ICRS becomes protected from mechanical stress, which might be
229 favorable for preventing keratoconus progression, if the implant is located close to the
230 focal weakening. Since the distribution of stress may be potentially different when two
231 segments of ICRS are implanted - instead of just one, as this study evaluated - this
232 same hypothesis might not be interchangeable in such a situation. Further studies are
233 needed to evaluate such a hypothesis.

234 Corneal tunnel creation alone did only cause few localized optical aberrations, which
235 were likely associated with epithelial defects. The fact that compressive strains in the
236 vicinity of the tunnel were independent of IOP increase or decrease indicates that
237 these strains likely resulted from tissue insult during manual tunnel creation. Manual
238 creation of corneal tunnel requires the use of a dissector that tears up the cornea along
239 a lamellar plane by rotating the dissector. Due to this local application of brute force,
240 it is reasonable to expect a longer lasting mechanical impact on neighboring tissue
241 that even outlasts the measurement period of the current study.

242 Interestingly, the induced sagittal curvature changes observed after ICRS implantation
243 were substantially higher (-19.3 diopters) than expected clinically (~ -6 diopters) for
244 long-arc ICRS dimensions^{17,18}. On one hand, this difference may be expected from
245 the fact that refractive corrections after ICRS implantation decrease within the initial
246 post-operative time. Assessment of the refractive state in clinical studies occurred as
247 early as 1-day post-operative¹⁹. Follow-up after 3 months showed that refractive
248 corrections became 13% less pronounced¹⁹, suggesting that corneal stroma and

249 epithelium undergo important remodeling after surgery. On the other hand, this
250 difference could be related to the fact that tunnel depth was slightly shallower (56 to
251 64%) in the current study than recommended in patients (70% to 75%). A numerical
252 study¹⁰ suggests that a more shallow implantation depth provokes a larger reduction
253 of spherical equivalent. An additional interesting point observed here was the
254 compressive strain induced at the outer edge of the ICRS, particularly during the IOP
255 increase. Clinically, such a compressive force could explain late extrusions and
256 recurrent epithelial erosions observed in cases where the rings are superficially
257 implanted.

258 This study is not exempt of limitations. First of all, the stromal tunnel was created
259 manually without access to a surgical microscope, which made it challenging to
260 achieve an appropriate tunnel depth and avoid corneal penetration. However, corneas
261 that had perforation were naturally excluded from this analysis. Second, the resulting
262 limited number of eyes that were successfully implanted and measured. Third, the fact
263 that healthy porcine eyes were investigated. Porcine corneas are reportedly^{15,16}
264 thicker than human corneas (factor ~1.7). The difference is even more pronounced
265 when considering ectatic (e.g. keratoconic) human corneas, in which thickness is
266 locally reduced and in which ICRS are typically implanted. Therefore, the strain
267 amplitude and strain pattern observed in the current study may result noticeably
268 different in those corneas. Future research is demanded to overcome these issues
269 and to quantify the induced strain field with different ICRS dimensions, arc lengths and
270 depths of corneal implantation, as well as in a disease model of corneal ectasia.

271 In conclusion, the current study proves the usefulness of OCE for the assessment of
272 the spatially highly-resolved strain field induced by additive surgery such as ICRS
273 implantation. In particular, we demonstrated that the corneal curvature map and the

274 axial strain field are directly related, which might open a new way to better understand
275 and predict the underlying mechanisms of ICRS surgery.

276

277

278 **Acknowledgement:**

279 This study received funding from the Swiss National Science Foundation (Ambizione
280 PZ00P2_174113 to SK). The authors thank Mediphacos (Belo Horizonte, MG, Brasil)
281 for sponsoring the intrastromal ring segments and the surgical kit required for
282 implantation.

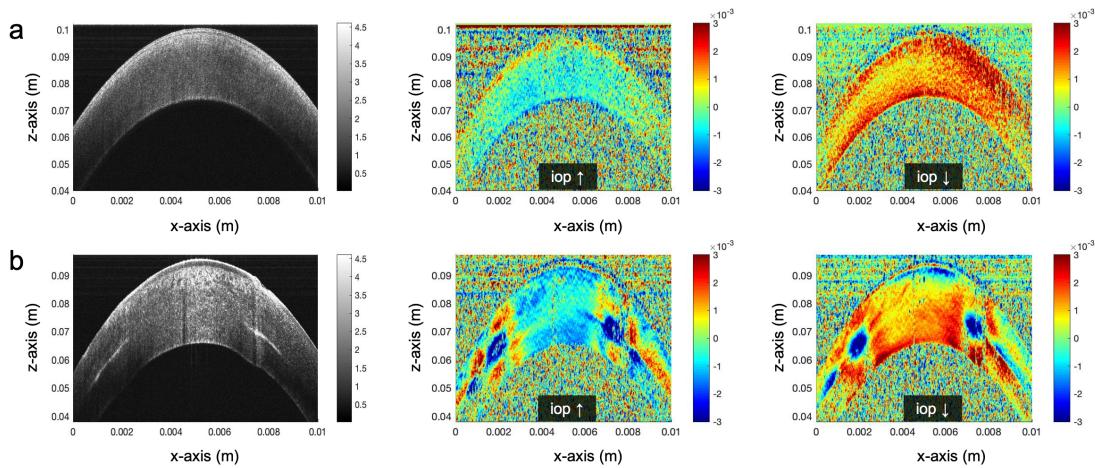
283 **References:**

- 284 1. Schanzlin, D. J., Asbell, P. A., Burris, T. E. & Durrie, D. S. The Intrastromal
285 Corneal Ring Segments: Phase II Results for the Correction of Myopia.
286 *Ophthalmology* **104**, 1067–1078 (1997).
- 287 2. Arriola-Villalobos, P. *et al.* Intrastromal corneal ring segment implantation for high
288 astigmatism after penetrating keratoplasty. *J. Cataract Refract. Surg.* **35**, 1878–
289 1884 (2009).
- 290 3. Miranda, D. *et al.* *Ferrara intrastromal corneal ring segments for severe*
291 *keratoconus*. (Slack Incorporated Thorofare, NJ, 2003).
- 292 4. Barraquer, J. I. Modification of refraction by means of intracorneal inclusions. *Int.*
293 *Ophthalmol. Clin.* **6**, 53–78 (1966).
- 294 5. Giacomini, N. T. *et al.* Intracorneal ring segments implantation for corneal ectasia.
295 *J. Refract. Surg.* **32**, 829–839 (2016).
- 296 6. Ruckhofer, J., Stoiber, J., Twa, M. D. & ünther Grabner, G. Correction of
297 astigmatism with short arc-length intrastromal corneal ring segments: preliminary
298 results. *Ophthalmology* **110**, 516–524 (2003).
- 299 7. Kubaloglu, A. *et al.* Intrastromal corneal ring segment implantation for the
300 treatment of keratoconus. *Cornea* **30**, 11–17 (2011).
- 301 8. Fernández-Vega Cueto, L. *et al.* Intrastromal corneal ring segment implantation
302 in 409 paracentral keratoconic eyes. *Cornea* **35**, 1421–1426 (2016).
- 303 9. Ariza-Gracia, M. Á., Flecha-Lescún, J., Büchler, P. & Calvo, B. Corneal
304 biomechanics after intrastromal ring surgery: Optomechanical in silico
305 assessment. *Transl. Vis. Sci. Technol.* **9**, 26–26 (2020).

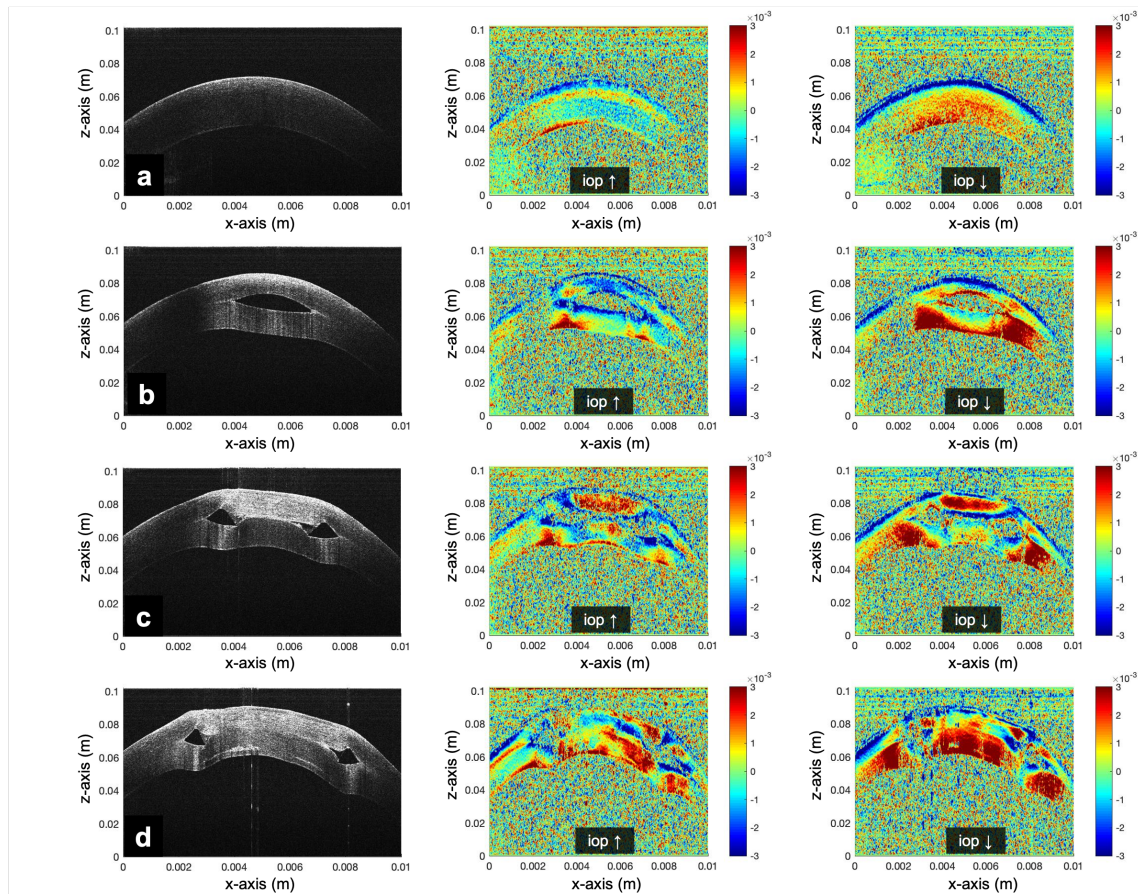
- 306 10. Ariza-Gracia, M. A., Flecha-Lescún, J., Calzada, B. C. & Büchler, P.
307 Biomechanically-driven simulations of the MyoRing treatment in subjects with
308 high myopia. *Invest. Ophthalmol. Vis. Sci.* **61**, 4722–4722 (2020).
- 309 11. Kling, S. & Marcos, S. Finite-element modeling of intrastromal ring segment
310 implantation into a hyperelastic cornea. *Invest. Ophthalmol. Vis. Sci.* **54**, 881–889
311 (2013).
- 312 12. Kling, S., Khodadadi, H. & Goksel, O. Optical Coherence Elastography-Based
313 Corneal Strain Imaging During Low-Amplitude Intraocular Pressure Modulation.
314 *Front. Bioeng. Biotechnol.* **7**, (2019).
- 315 13. Kling, S., Torres-Netto, E. A., Spuru, B., Sekundo, W. & Hafezi, F. Quasi-static
316 optical coherence elastography to characterize human corneal biomechanical
317 properties. *Invest. Ophthalmol. Vis. Sci.* **61**, 29–29 (2020).
- 318 14. Kling, S. Optical coherence elastography by ambient pressure modulation for
319 high-resolution strain mapping applied to patterned cross-linking. *J. R. Soc.*
320 *Interface* **17**, 20190786 (2020).
- 321 15. Sanchez, I., Martin, R., Ussa, F. & Fernandez-Bueno, I. The parameters of the
322 porcine eyeball. *Graefes Arch. Clin. Exp. Ophthalmol.* **249**, 475–482 (2011).
- 323 16. OLSEN, T. & EHLERS, N. The thickness of the human cornea as determined by
324 a specular method. *Acta Ophthalmol. (Copenh.)* **62**, 859–871 (1984).
- 325 17. Izquierdo Jr, L., Rodríguez, A. M., Sarquis, R. A., Altamirano, D. & Henriquez, M.
326 A. Intracorneal circular ring implant with femtosecond laser: Pocket versus
327 tunnel. *Eur. J. Ophthalmol.* 1120672121994729 (2021).
- 328 18. Sadoughi, M. M. *et al.* Femtosecond laser implantation of a 340-degree
329 intrastromal corneal ring segment in keratoconus: short-term outcomes. *J.*
330 *Cataract Refract. Surg.* **43**, 1251–1256 (2017).

331 19. Michael, R. *et al.* Refractive and biomechanical changes with intrastromal ring
332 segments for keratoconus. *Acta Ophthalmol. Scand.* **85**, (2007).
333
334

335 **Figures:**
336

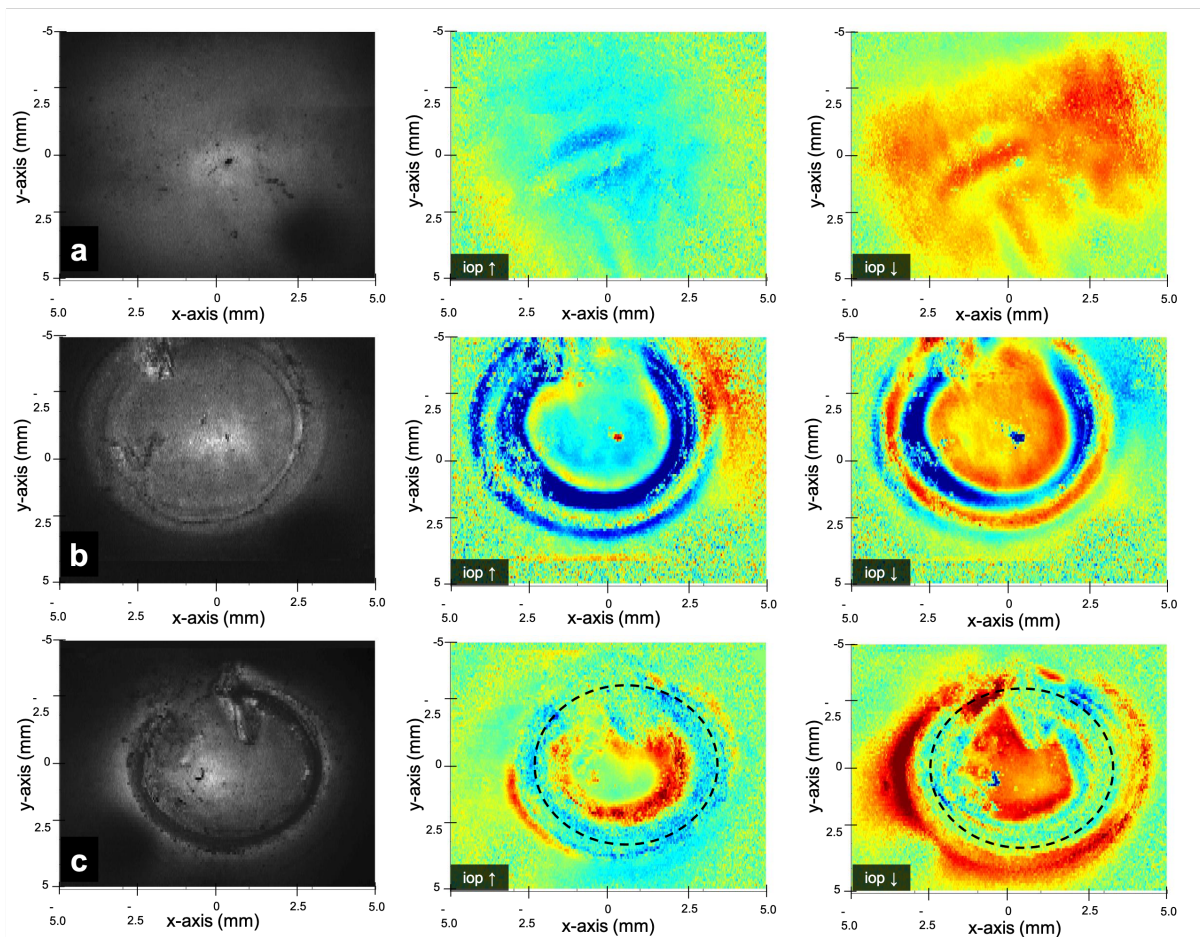


337
338 **Figure 1.** Cross-sectional view of standard structural imaging (left panel) and strain
339 imaging (a) in a virgin cornea, (b) after tunnel creation, during IOP increase (middle
340 panel) and IOP decrease (right panel). Red color means positive axial strain (i.e.
341 relaxation), blue color means negative axial strain (i.e. compression). Predominantly,
342 axial compressive strains are observed during IOP increase and axial tensile strains
343 during IOP decrease. After tunnel creation, localized compressive strains occurred in
344 the direct vicinity of the tunnel.
345

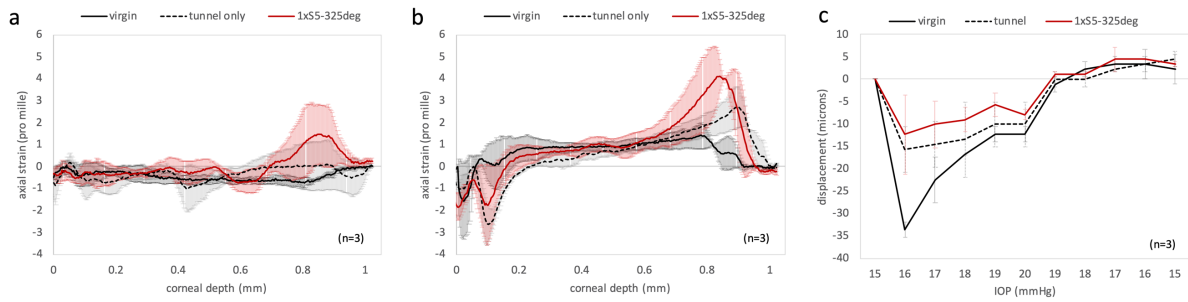


346
347 **Figure 2.** Cross-sectional view with standard structural imaging (left panel) and strain
348 imaging after ICRS (300 μ m thickness, arc length 325 $^\circ$) implantation at different

349 locations of the cornea from periphery (top line) to center (bottom line), during IOP
 350 increase (middle panel) and IOP decrease (right panel). Red color means positive
 351 axial strain (i.e. relaxation), blue color means negative axial strain (i.e. compression).
 352 The panels a-d represent different locations on the cornea: at direct vicinity of the
 353 corneal tunnel (panel a), the outer edge of the ICRS (panel b), at approx. $\frac{1}{4}$ of the
 354 ICRS (panel c) and at a higher distance between arcs (panel d). ICRS implantation
 355 introduced tensile strains located in the anterior cornea at the inner edge of the
 356 segment, but hardly affected tissue strains in the periphery of the segment. The
 357 implant also induced some localized strains in its direct vicinity.
 358

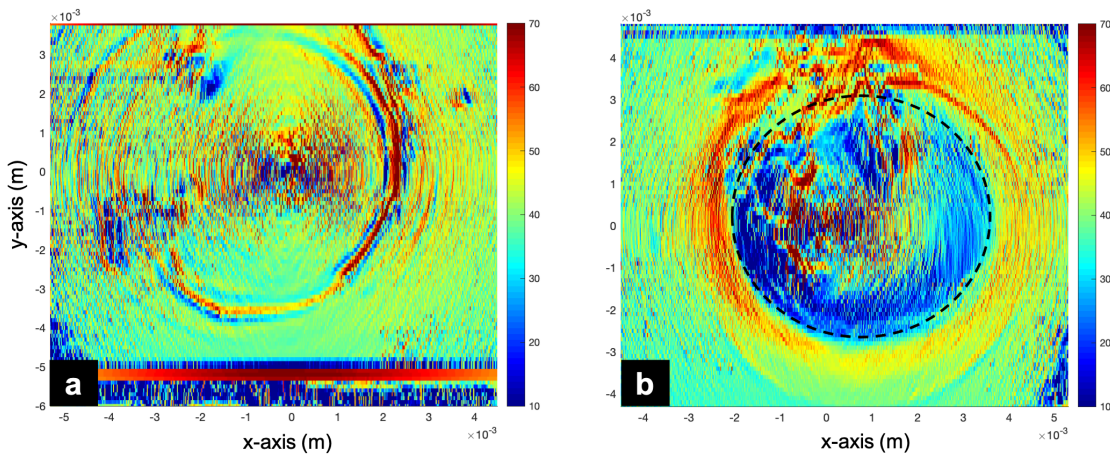


359 **Figure 3.** Enface view with standard structural imaging (left panel) and strain imaging
 360 in (a) a virgin cornea, (b) after tunnel creation, (c) after ICRS (300 μ m thickness, arc
 361 length 325 $^{\circ}$) implantation, during IOP increase (middle panel) and IOP decrease (right
 362 panel). Dashed circles are a reference for comparison with Figure 5. Red color means
 363 relaxation, blue color means compression. After ICRS implantation a second ring of
 364 positive strain (red color) was observed at the inner edge of the ICRS, indicating
 365 localized tissue relaxation.
 366
 367



368
369
370
371
372
373
374
375
376

Figure 4. Axial strain profile in the central optical zone of 4mm diameter. **(A)** During IOP increase. Without an ICRS, strain amplitudes are mostly small and of compressive nature. With an ICRS, a trend towards tissue relaxation in the posterior cornea is observed. **(B)** During IOP decrease. Generally larger strain amplitudes are observed. With an ICRS, the posterior cornea demonstrated a significantly increased tissue relaxation. **(C)** Axial displacement. With an ICRS, the smallest displacement was observed.



377
378
379
380
381
382
383
384
385
386
387
388
389
390
391
392

Figure 5. Sagittal curvature map of the cornea with **(A)** tunnel creation only, **(B)** ICRS implantation. The dashed circle is a reference for comparison with Figure 3. Substantial corneal flattening was observed interior to the ICRS and localized corneal steepening in the direct periphery of the ICRS.

Table 1. Overview of axial strain in the 80% anterior and 20% posterior corneal stroma, both during IOP increase and decrease. Central refers to the region interior (i.e. the optical zone) of the ICRS. comp. = compressive (negative) strains; relax. = tensile (positive) strains

		IOP↑		IOP↓	
		central	periphery	central	periphery
virgin	ant				
	post	comp.	comp.	relax.	relax.
	ant	comp.	comp.	relax.	relax.

tunnel- only	post	comp.	comp.	relax.	relax.
ICRS	ant	comp.	comp.	relax.	relax.
	post	relax.	comp.	relax.↑	relax.

393
394
395
396
397
398